

VARIANCE CONTROLLED SHEAR STIFFNESS IMAGES FOR MRE DATA

J Mclaughlin[†], *D Renzi*[†], *J R Yoon*[‡]

[†]Rensselaer Polytechnic Institute
Math Department
110 8th street, Troy, NY 12180

[‡]Clemson University
Department of Mathematical Sciences
Clemson, SC 29634-0975

R L Ehman, A Manduca

Mayo Clinic and Foundation
200 First Street SW, Rochester, MN 55905

ABSTRACT

In the Magnetic Resonance Elastography experiment we consider a harmonically oscillating mechanical force applied to the boundary surface of a phantom and synchronized with the motion encoding gradient. The phantom is symmetric in the direction of the applied mechanical force and the vector component in that direction decouples from the other components and satisfies a Helmholtz equation. We present a local inversion method to determine the shear wave speed that: (1) treats the phase and amplitude of the data differently; (2) computes derivatives of the data by using statistically justified filtering; and (3) varies filters according to SNR. We test our methods on data from Mayo Clinic and recover the position and stiffness of a 3mm diameter inclusion.

1. INTRODUCTION

Manual palpation has long been used by doctors to detect abnormal tissue by identifying stiff inclusions in soft tissue. The goal of elastography is to replace the subjective manual palpation exam with a quantitative image of shear stiffness. Magnetic Resonance Elastography (MRE), [2, 4, 5, 6, 7, 9, 11, 14], is one proposed technique to generate these shear stiffness images. In MRE, the vector displacement of a time harmonic wave is measured as a function of space and time. For symmetric phantoms, the component along the symmetric axis decouples and can be shown to satisfy the Helmholtz equation for the shear wave only. The shear modulus or shear wave speed is obtained by inversion of this equation. Many direct techniques have been proposed to accomplish this inversion, including phase conjugation, direct inversion, low frequency estimation, and matched filter, see [6, 7] for a comparison of these methods. While these techniques have been very successful in reconstructing stiffness images, we note that the variance in the final image can vary substantially in low and high signal regions.

In this paper we develop a new technique for inverting the Helmholtz equation to find the ratio of the shear modulus to the density, i.e., the square of the shear wave speed, to be applied when a single component satisfies this equation. In this technique we will treat the phase and amplitude of the displacement separately using a local averaging scheme, [1], to directly calculate the derivatives in the Helmholtz equation. What differentiates our scheme from the other direct inversion schemes is that our scheme will use spatially varying smoothing filters designed to equalize the variance across the final image. To accomplish this we first separate the complex displacement (Fourier transformed real displacement data) into phase and amplitude. With this decomposition, the Helmholtz equation contains both first derivative and second derivative terms of the phase and amplitude to which we apply different smoothing filters. This eliminates over smoothing of the information rich first derivative terms. We will also use an adaptive amount of smoothing based on the local signal to noise ratio (SNR). This will allow the recovery of very small inclusions in high SNR regions without the introduction of artifacts in low SNR regions. The matched filter, [10], also is an adaptive filter. This filter is designed to locally minimize the variance, but the variance can differ substantially across the image.

The rest of this paper is composed as follows. The governing equations are described in Section 2. Next, our inversion technique is given in section 3. A reconstruction from a phantom experiment performed at the Mayo Clinic is given in Section 4. Finally, we give some concluding remarks in section 5.

2. THEORY

In MRE, a mechanical oscillation is synchronized with a motion encoded magnetic gradient. Measurements are taken with two polarizations of the motion encoded magnetic gradient. The phase difference between the two measurements is pro-

portional to the displacement in the direction of the motion encoded magnetic gradient, see [2]. Repeating the experiment with the motion encoding gradient in three different orthogonal directions yields a very rich 3D data set of the displacement of a time harmonic wave measured as a function of space and time. The induced displacements are very small (on the order of microns), so a linear model is appropriate. Since stiffness is an elastic property, the proper model is the linear equations of elasticity. In the model we consider, the phantom has two cylindrical inclusions, one with 16mm diameter, the other with a 3mm diameter. The axes of the cylinders and the direction of the harmonic surface excitation are parallel. In this case the elastic displacement in this same direction decouples from the other two components and varies only in the two orthogonal directions. The Fourier transform, u , of this component of the elastic displacement satisfies the Helmholtz equation:

$$\nabla \cdot (\mu(x)\nabla u) = -\omega^2 \rho u, \quad (1)$$

where μ , ρ , and ω are the shear modulus, density, and frequency of excitation.

3. INVERSION ALGORITHMS

For our inversion algorithms we use a direct inversion technique, which requires us to assume that μ is locally constant. This is a very common assumption, see for example, [2, 4, 5, 6, 7, 9, 11]; validation of this assumption has primarily been in phantoms whose material properties are piecewise constant. Continuing, in our method we first let $u = M e^{i\phi}$, where $M = |u|$ is the amplitude and $\phi = \text{angle}(u)$ is the phase. Now, substitution into (1) along with the locally constant assumption yields

$$\omega^2 \rho M = \mu(x)(M|\nabla\phi|^2 - \Delta M - i(2\nabla M \cdot \nabla\phi + M\Delta\phi)). \quad (2)$$

Solving for μ/ρ yields

$$\frac{\mu}{\rho}(x) = \frac{M\omega^2}{(M|\nabla\phi|^2 - \Delta M - i(2\nabla M \cdot \nabla\phi + M\Delta\phi))}. \quad (3)$$

In this paper we use equation (3) and image the quantities $\text{Re}(\mu/\rho)$ and $|\mu/\rho|$. To achieve our goal we only have to estimate $|\nabla\phi|$, ΔM , $\nabla M \cdot \nabla\phi$, and $\Delta\phi$. Below, we describe our algorithm.

3.1. Inversion Algorithm

Our algorithm is based on the numerical differentiation scheme given in [1]. With the appropriate choice of parameters, this scheme is essentially a centered difference approximation to the derivative, with each point in the centered difference stencil replaced with a local average. In our implementation the local average is taken over a square centered at the point in the difference stencil whose sides are equal in length to half

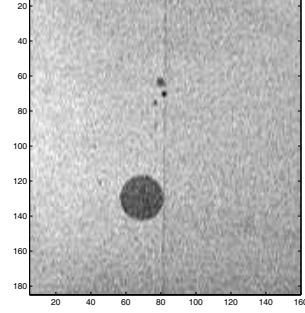


Fig. 1. Phantom cross section; The height and length of the imaging plane are 102mm and 97mm.

of the step size. The step size is the regularization parameter, γ , and controls the tradeoff between accuracy and smoothness of the derivative. This algorithm is used to calculate all the derivatives in equation(3), applying the algorithm twice to calculate the second derivative terms, but varying the step size. It is not surprising that, without taking special care, the second derivatives terms are noisier than the first derivative terms, and that all terms are noisier in low SNR regions than high SNR regions. The philosophy behind our algorithm is to produce an image where the variance is approximately equal across the image. With this in mind, we use a larger regularization parameter for the second derivative terms, calculate either $\text{Re}(\mu/\rho)$ or $|\mu/\rho|$, and then median filter the result using an $s \times s$ window, where s is adjusted according to the SNR. In a later paper we will demonstrate that this method produces an image with constant variance across the medium. Finally, we post-process the image by minimizing the total variation, [13], which is well known to preserve large contrasts. Use of total variation minimization allows one to use smaller regularization parameters in the rest of the algorithm, which leads to less bleeding around the edges of the inclusions.

4. PHANTOM RESULTS

Here we give our results on a phantom experiment performed at the Mayo Clinic on an approximately rectangular gel phantom. The phantom contains two smaller cylinders of stiffer gel. The diameters of the cylinders are approximately 16 mm and 3 mm respectively. A cross section of this phantom is shown in Figure 1. A major goal of this paper is to image the 3 mm inclusion. The shear modulus and density have been previously estimated, [12], by creating homogeneous phantoms of the same material contained in the background and in the stiff cylindrical inclusions with low frequency estimation. The shear modulus is approximately 20 kPa in the background and approximately 130 kPa in the stiff inclusions and the density is approximately 1000 kg/m³. A mechanical excitation induces a harmonic oscillation at the surface in a direction parallel to the axes of the cylinders. As de-

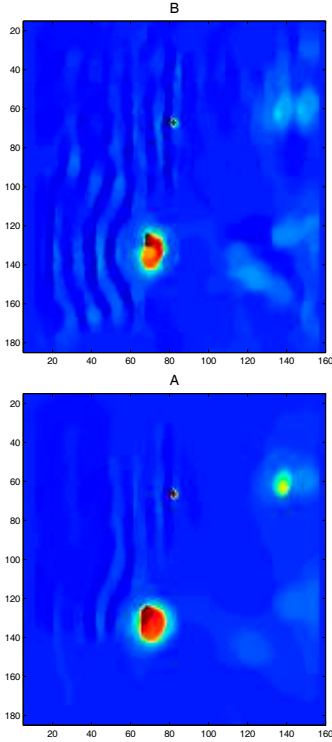


Fig. 2. Images of: A $\text{Re}(\mu/\rho)$ and B $|\mu/\rho|$ using variance control showing well imaged small 3mm inclusion; $\gamma_1 = 3, \gamma_2 = 6$, using an $s \times s$ window for the median filter, where s varies according to the SNR; post processing with TV filter;

scribed above, in this case the Fourier transform of the elastic displacement in this same direction decouples from the other two components and satisfies the Helmholtz equation.

We use the direct inversion algorithm described above with the following parameters: (1) the regularization parameter for the second derivative terms is $\gamma_2 = 6$; (2) the regularization parameter for the first derivative terms is $\gamma_1 = 3$; (3) the window size used for the median filter, $s \times s$, varies between 7×7 and 15×15 pixels and is inversely proportional to the SNR. With these parameters we calculate $\text{Re}(\mu/\rho)$ and $|\mu/\rho|$. These images are shown in Figure 2 A, B. In each case, the small and large inclusions are clearly visible. In particular, the amplitude of the small inclusion has been correctly computed. There is a small artifact with a significant amplitude near the upper right edge of the medium. The cause of this artifact is that there is a long thin low signal area in this place. Our SNR estimate is calculated using a square region, so the SNR is overestimated in this region. There are also some very low amplitude artifacts in the wake behind the large inclusion, though the artifacts are considerably smaller in amplitude than the stiff inclusions and in particular are barely noticeable in the image of $|\mu/\rho|$. The amplitude of the displacement, $M(x)$, is shown in Figure 3 A, where we see that

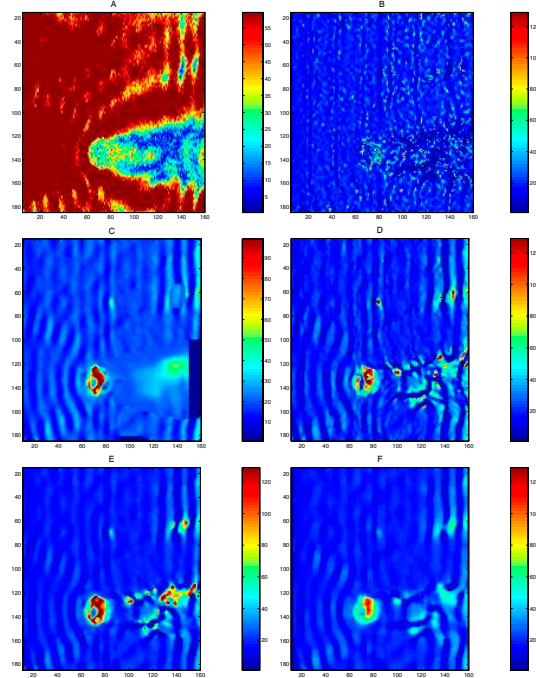


Fig. 3. A Amplitude $M(x)$; and instructional images exhibiting the importance of variance control: B $|\mu/\rho|$ using $\gamma_1 = \gamma_2 = 3$, and an SNR varied $s \times s$ window for the median filter. C $|\mu/\rho|$ using $\gamma_1 = \gamma_2 = 6$, and an SNR varied $s \times s$ window for the median filter. D $|\mu/\rho|$ using $\gamma_1 = 3, \gamma_2 = 6$, and a 7×7 window for the median filter. E $|\mu/\rho|$ using $\gamma_1 = 3, \gamma_2 = 6$, and an 11×11 window for the median filter. F $|\mu/\rho|$ using $\gamma_1 = 3, \gamma_2 = 6$, and a 15×15 window for the median filter. In C-F, post processing is done with a TV filter;

the small artifacts in Figure 2 appear to be in regions of very small amplitude. In the remaining images in Figure 3 we demonstrate the positive features of our algorithm: (1) using separate regularization parameters for the second derivative and first derivative terms; (2) using separate filters for high and low SNR regions; (3) separating the displacement into phase and amplitude. First, we calculate $|\mu/\rho|$ with the $\gamma_1 = \gamma_2$. Figure 3 B shows the result when $\gamma_1 = \gamma_2 = 3$ and Figure 3 C shows the result when $\gamma_1 = \gamma_2 = 6$. In both images the window size of the median filter varies with the SNR. Clearly Figure 3 B is too noisy to be useful. The noise in the second derivative terms destroys the image. While Figure 1 C is a reasonably good reconstruction, the small inclusion is very difficult to see. Note that the color bar has been changed in this figure to make the small inclusion visible. This demonstrates the value in the first feature of our algorithm. Note that we can only achieve this benefit through feature (3), separating the displacement into phase and amplitude. Second, we calculate $|\mu/\rho|$ using a fixed window size for the median filter.

In Figures 3 D, E, F we show the results using a 7×7 , 11×11 , and 15×15 pixel window. In Figure 3 D the small inclusion is reconstructed very well, but the large inclusion is not well resolved and there are a large number of artifacts of comparable size and amplitude to the small inclusion. Comparing with Figure 3 A, it appears that these artifacts are all in low SNR regions. In Figure 3 E, the amplitude of the small inclusion has been greatly reduced, and there are still artifacts in the low SNR regions. However, the large inclusion is reconstructed rather well. In Figure 3 F the artifacts have disappeared, but so has the small inclusion and the amplitude of the large inclusion has dropped. Note that Figure 2 B is essentially a combination of the best parts of Figures 3 D, E, and F. This demonstrates the value of the second feature of our algorithm. Similar improvements are obtained for $\text{Re}(\mu/\rho)$.

5. CONCLUSION

We treat MR time harmonic displacement data; measurements are at eight equally spaced times in the period of the harmonic cycle. Data acquisition is with the Mayo Clinic MRE system. Separation of displacement into phase and amplitude enables treating these two quantities separately with consistent variance controlled smoothing based on the order of derivative and the SNR ratio. This enables substantially improved, compare with [12], recovery of small 3mm diameter stiff inclusions with the correct stiffness amplitude, which is the target of this paper. The reader may also want to compare with [7]. There the smallest inclusion is 5mm in diameter with a contrast ratio of about 2.2 and a excitation frequency of 100Hz. Here the small inclusion has a diameter of 3mm with a contrast ratio of about 6 and an excitation frequency of 300Hz. Here we correctly determine the amplitude of the shear modulus μ in the small inclusion.

6. REFERENCES

- [1] Anderssen R S and Hegland M 1999 For numerical differentiation, dimensionality can be a blessing! *Mathematics of Computation* **68** n 227 1121-41
- [2] Braun J, Buntkowsky G, Bernarding J, Tolxdorff T, and Sack I 2001 Simulation and analysis of magnetic resonance elastography wave images using coupled harmonic oscillators and Gaussian local frequency estimation *Magnetic Resonance Imaging* **19** 703–13
- [3] Greenleaf J F, Muthupillai R, Rossman P J, Smith J, Manduca A and Ehman R L 1996 Direct visualization of strain waves by magnetic resonance elastography (MRE) 1996 *IEEE Ultrasonics Symposium Proceedings* **1** 467-72
- [4] Kruse S A, Smith J A, Lawrence A J, Dresner M A, Manduca A, Greenleaf J F, and Ehman R L 2000 Tissue characterization using magnetic resonance elastography: preliminary results *Physics in Medicine and Biology*, **45** 1579–90
- [5] Manduca A, Oliphant T E, Dresner M A, Mahowald J L, Kruse S A, Amromin E, Felmlee J P, Greenleaf J F, and Ehman R L 2001 Magnetic resonance elastography: Non-invasive mapping of tissue elasticity *Medical Image Analysis* **5** 237–54
- [6] Manduca A, Oliphant T E, Lake D S, Dresner M A, and Ehman R L 2002 Characterization and evaluation of inversion algorithms for MR elastography *Proceedings of the SPIE - The International Society for Optical Engineering* **4684** pt.1-3 1180-5
- [7] Manduca A, Lake D S, and Ehman R L 2003 Spatio-Temporal directional filtering for improved inversion of MR Elastography Images *Medical Image Analysis* **7** 465-473
- [8] Manduca A, Muthupillai R, Rossman P J, and Greenleaf J F 1996 Image processing for magnetic resonance elastography *Proceedings of the SPIE - The International Society for Optical Engineering* **2710** 616-23
- [9] Muthupillai R, Lomas D J, Rossman P J, Greenleaf J F, Manduca A, and Ehman R L 1995 Magnetic resonance elastography by direct visualization of propagating acoustic strain wave *Science* **269** 1854–57
- [10] Oliphant T E, Kimmick R R, Manduca A, Ehman R, Greenleaf J F 2000 An error analysis of Helmholtz inversion for incompressible shear, vibration elastography with application to filter design for tissue characterization 2000 *IEEE Ultrasonics Symposium* 1795-98
- [11] Oliphant T E, Manduca A, Ehman R, Greenleaf J F 2001 Complex-valued stiffness reconstruction for magnetic resonance elastography by algebraic inversion of the differential equation. *Magnetic Resonance in Medicine* **45** 299-310
- [12] Romano A J, Bucaro J A, Ehman R L, Shirron J J 2000 Evaluation of a material parameter extraction algorithm using MRI-based displacement measurements *IEEE Transactions on Ultrasonics, Ferroelectrics and Frequency Control*, v 47, n 6, Nov. 2000, p 1575-81 **47** n 6 1575-81
- [13] Rudin L I, Osher S, Fatemi E 1992 Nonlinear total variation based noise removal algorithms *Physica D* **60** 1-4 259-68
- [14] Van Houten E E W, Paulsen K D, Miga M I, Kennedy F E, and Weaver J B 1999 An overlapping subzone technique for MR-based elastic property reconstruction *J. Acoust. Soc. Am.* **111** 439–46